ACS APPLIED MATERIALS & INTERFACES

Research Article

www.acsami.org

In Situ Polymerization Deposition of Porous Conducting Polymer on Reduced Graphene Oxide for Gas Sensor

Yajie Yang, Shibin Li,* Wenyao Yang, Wentao Yuan, Jianhua Xu, and Yadong Jiang

State Key Laboratory of Electronic Thin Films and Integrated Devices, School of Optoelectronic Information, University of Electronic Science and Technology of China (UESTC), Chengdu 610054, People's Republic of China

ABSTRACT: Porous conducting polymer poly(3,4-ethylenedioxythiophene) (PEDOT) nanocomposite prepared on reduced graphene oxide (RGO) film was used as efficient chemiresistor sensor platform for NO_2 detection. The comparable electrical performance between RGO and porous PEDOT nanostructure, the large surface area and opening porous structure of this RGO/porous PEDOT nanocomposite resulted in excellent synergistic effect. The gas sensing performance revealed that, in contrast to bare RGO, the RGO/porous PEDOT exhibited the enhanced sensitivity (2 orders of magnitude) as well as response and recovery performance. As a result of the highly uniform distribution of PEDOT porous network and excellent synergetic effect between RGO and porous PEDOT, this nanocomposite based sensor exhibited higher selectivity to NO_2 in contrast to other oxidant analyte gases, e.g., HCl, H_2S and SO_2.

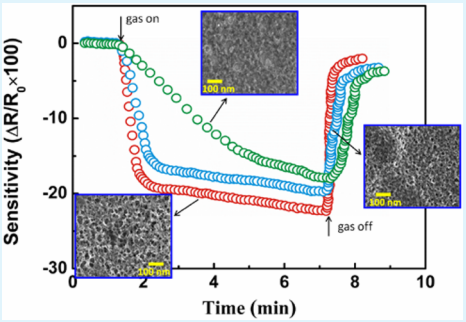

KEYWORDS: *reduced graphene oxide, conducting polymer, LB films, porous nanostructure, gas sensors*

1. INTRODUCTION

As one specific branch of graphene research, the study of graphene oxide (GO) and GO based materials has been popular and extensive in recent years.[1,2] Compared with pristine graphene, the covalent oxygenated functional groups in GO can indeed give rise to remarkable structure defects.[3] The presence of these functional groups also provides potential advantages for using GO in numerous applications.[4,5] These functional groups serve as sites for chemical modification or functionalization of GO, which, in turn, can be employed to immobilize various electroactive species through covalent or noncovalent bonds for the design of sensitive chemical and electrochemical systems.[6−10]

The easy synthesis and solution processability have made GO a very attractive material for nanocomposite and graphene-related electronics applications.[11−16] By controlling the structural disorder, GO can be made into an insulating, semiconducting, or semimetallic material by appropriately fine-tuning the oxidation or reduction parameters.[17−20] As a reduction product of GO, reduced graphene oxide (RGO) resembles graphene, but with some residual oxygen and structural defects, yielding a conductivity that is comparable to that of doped conductive polymers.[21,22] So, the composites based on RGO and conducting polymer show good synergetic effects to improve performance.[23−25] The tunable electrical performance of RGO also makes it a promising functional material.[26−28] The first gas sensor based on graphene was reported by Novoselov et al.[29] Chemically reduced graphene oxide sheets have also shown promising applications for gas sensors as well.[30−32] Moreover, the improved conductive performance and defective nature of RGO indicate very different chemical reactivity compared to graphene and GO, and make them suitable for high sensitivity gas sensors.[33−36] Recently, RGO has attracted much attention for use as a chemiresistor, due to its scalable production, solution processability, large available surface area, etc.[37,38] Although many papers reported the sensing properties of RGO, it is still a great challenge to develop the sensing devices based on RGO to improve sensitivity and selectivity.

Conducting polymers and their nanostructures, as excellent sensing materials, have been extensively studied because of their high sensitivities, excellent reliability and low cost properties.[39−41] Hybridization of a conducting polymer with GO and RGO has been studied and demonstrated enhancement in sensitivity and selectivity of a gas sensor compared with pure GO and RGO sensors.[42−46] It has been demonstrated that a conducting polymer, especially the nanostructured conducting polymer, plays important roles in enhancement of the sensing performance of GO and RGO devices.[47,48] However, limited articles have reported gas sensors based on the single layer RGO and porous conducting polymer nanostructures. It is expected that the decoration of a porous conducting polymer nanostructure on the surface of RGO can greatly improve the sensitivity and selectivity of the pure RGO based sensor, through combination of both excellent sensing materials. Therefore, we demonstrate a NO_2 gas sensor based on RGO and the porous conducting polymer poly(3,4-ethylenedioxythiophene) (PEDOT) nanostructure. The single layer RGO

Received: May 23, 2014
Accepted: July 30, 2014
Published: July 30, 2014

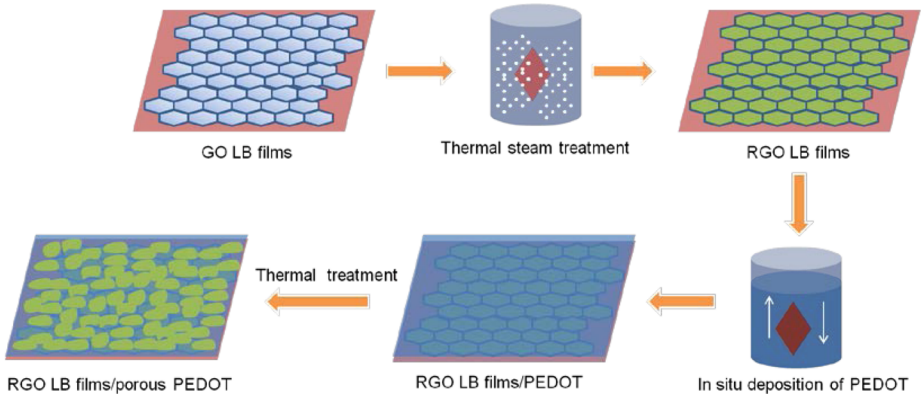

Figure 1. Schematic illustration of preparing RGO/porous PEDOT nanocomposite.

film is obtained from the GO Langmuir–Blodgett deposition and a subsequent thermal reductive treatment. The porous PEDOT nanostructure has been successfully deposited on the surface of RGO sheets by using a fast thermal treatment during the in situ polymerization of 3,4-ethylenedioxythiophene (EDOT) monomer. The resultant RGO/porous PEDOT nanocomposite has been studied as excellent sensing materials for the detection of NO_2 gas.

2. EXPERIMENTAL SECTION

2.1. Materials. Graphite flakes used for GO preparation were purchased from Sigma-Aldrich. GO was synthesized from natural graphite flakes prepared through the Hummers' method.[49] The size of graphite flakes was 380 μm (grade 3061) and 40 μm (grade 230). To obtain stable GO dispersion for LB deposition, 20 mg of GO was dissolved in 80 mL of methanol/DI water (volume ratio 4:1) mixture solution, and the solution was subjected to ultrasonication for 30 min followed by centrifugation at 2500 rpm. EDOT (3,4-ethylenedioxythiophene) monomer and oxidizer Iron(III) *p*-toluene sulfonate hexahydrate ($(Fe(PTS)_3$) were purchased from Bayer Company. All chemical solvents in experiments were high purity grade.

2.2. Preparation of Single Layer RGO. Single layer GO sheets deposition was carried out in KSV-5000 LB system. The trough was carefully cleaned with chloroform and then filled with DI water. The GO solution was dropwise spread onto the water surface using a glass syringe. Surface pressure was monitored using a tensiometer attached to a Wilhelmy plate. The film was compressed by barriers at a speed of 1 mm/min. The GO monolayer was transferred to substrates at various points during the compression by vertically dipping the substrate into the trough and slowly pulling it up (1 mm/min). The substrate was first processed with a hydrophilic treatment to deposit uniform GO LB layers. After the GO LB film deposition, the single GO layer covered substrate was treated in a water vapor oven at 180 °C for 4 h of GO reduction.[36]

2.3. Preparation of Porous PEDOT on RGO. As shown in Figure 1, in situ polymerization solution of PEDOT was prepared by introducing 4.5 mL of EDOT (3,4-ethylenedioxythiophene) into 50 mL of an *n*-butyl alcohol and acetone mixed solution (volume ratio 1:1). After a thorough stirring, 1.5 mL of $Fe(PTS)_3$ was introduced into the EDOT solvent mixture to trigger the polymerization of EDOT. This in situ polymerization solution was kept at 5 °C for low speed polymerization. Then, the RGO covered substrate was immersed into the PEDOT solution by dip-coating process for an in situ deposition of the PEDOT layer. This dropping in and out process was carried out in a KSV dip-coater to form an ultrathin PEDOT layer. To obtain the uniform PEDOT layer for sensing performance comparison, the PEDOT layers with 80–110 nm thickness were formed on RGO at a slow dipping speed (0.5 m/min). Then, the RGO/PEDOT covered substrate was quickly transferred into a room temperature oven for a fast rate baking treatment. The oven temperature increased from room temperature to 80 °C at 15 °C/30 s, and the substrate was successively kept at 80 °C in an oven for 30 min. After the baking process of PEDOT for 30 min, the product was washed by ethanol to remove residual reagent.

2.4. Characterization. The UV–vis-near IR (UV–vis-NIR) spectrum of the film was recorded on a UV 1700 spectrometer (SHIMADZU). The Fourier transform infrared spectroscopy (FT-IR) spectrum was characterized with an ALPHA analysis instrument (Germany). The surface pressure–area (π–A) isotherm recorded by computer and the morphology analysis of GO sheets at air–water interface was characterized by a Brewster angle microscope (BAM 300). The surface morphology of GO and RGO film was investigated by atomic force microscopy (AFM, Model SP 3800, SII, Japan) with a tapping mode. The morphological properties of RGO/porous PEDOT were investigated with scanning electron microscopy (SEM), using a Hitachi scanning electron microscope (Model S-2400). The current–voltage (I–V) curves of GO and RGO were obtained by using a Keithley semiconducting testing system (Model 4200).

The RGO/PEDOT film was prepared across an interdigitated electrode to test gas sensitivity in an airtight chamber. A conventional photolithographic method was used to fabricate the interdigitated electrode with a finger width of 30 μm and a gap size of 20 μm. The electrodes (30 nm Ti and 50 nm Au) were thermally evaporated on a layer of silicon dioxide (SiO_2). The sensor was placed inside a stainless chamber of 60 mL volume, which was kept under continuous flowing of testing gas mixtures or air at a constant flow rate of 100 mL min^{-1}. NO_2 gas with concentrations from 500 ppb to 20 ppm was utilized to evaluate the sensing performance. Prior to the measurement, the interdigitated electrode was blown with dry N_2 flow and the corresponding vapor was injected into a gas chamber. The resistance was monitored continuously over time. For a selectivity test, the dynamic mixed gases were injected into a gas chamber through a homemade gas distribution system. The analytic gases with different concentrations were generated by mixing saturated vapors with dry air controlled by mass flow controllers. The resistance change of RGO/porous PEDOT film and RGO film based sensors were monitored with a computer controlled source meter (Keithley 2400). The sensitivity of the sensor was monitored by applying a constant bias voltage of 1.2 V on the sensor and recording the conductance change. All the gas sensing measurements were performed at ambient temperature (23 °C), and the humidity of testing system was kept below the 15% relative humidity (RH) in a dynamic test.

3. RESULTS AND DISCUSSION

In our work, a single layer GO LB film has been first introduced on a substrate and successive thermal treatment is utilized to form single layer RGO. The successively formed RGO layer not only can be utilized as high performance sensing layer but also can afford high surface area for in situ polymerization deposition of PEDOT. As a single atomic layer carbon sheet, GO contains a large and flexible sheet structure, which shows geometric similarity with the air–water interface. So, GO can

float on a water surface without surfactants or stabilizing. Figure 2 shows the surface pressure−area (π−A) curve of GO layers at

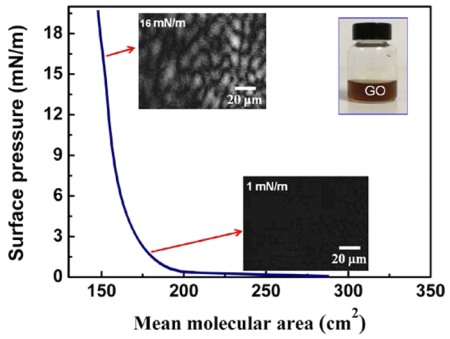

Figure 2. surface pressure-mean molecular area (π−A) isotherm curves of GO at air−water interface. The inset pictures show the BAM images of GO at different surface pressures and a GO dispersion solution for LB deposition.

the air−water interface. The curve indicates that GO sheets can arrange compactly at the air−water interface with continuous compression of barriers to high surface pressure. This compact GO sheets arrangement at the air−water interface can be deposited on different substrates through vertical or horizontal LB deposition, and single layer and highly compact GO sheets can be obtained for different applications.

By controlling the surface pressure, surface coverage of the graphene oxide sheets is manipulated to realize a uniform deposition with compact and incompact arrangements. Moreover, large area LB deposition can also be realized on GO sheets with a tunable arrangement on different substrates for varied functional applications. In this work, the single layer and compact arrangement GO sheets are deposited on the substrate. Due to the excellent manipulation of GO LB deposition on different substrates, we intend to introduce this GO LB layer to form a compact and large area RGO layer after reductive treatment, and a porous conducting polymer nanostructure can be constructed on the latter formed RGO layer as a novel nanocomposite.

Covalent oxygenated functional groups in GO can indeed give rise to remarkable structure defects in the carbon sheet, leading to low conductivity of GO. Due to the low conductivity, pure GO is not suitable as a carries transportation layer and a further reductive treatment on GO would lead to the formation of RGO with better conductive characteristics. To keep the original morphology of single layer GO LB films deposited on a substrate, we choose a thermal treatment in a water vapor environment as an efficient reduction process to obtain highly compact RGO sheets.[36] Figure 3a shows AFM images of single layer GO LB sheets deposited on a substrate. It can be seen that a highly compact arrangement of GO sheets is obtained through the LB deposition. The slight overlapping of GO sheets is observed in this single layer GO sheet (as shown by arrow in Figure 3a,b), and we deduce this result from sheets overlapping during the constant compressing of GO sheets at high surface pressures. After the thermal reductive treatment, compared with as-prepared GO layer, the obtained single layer RGO sheets can keep ordered and compact formation from GO LB films (as shown in Figure 3b). The excellent covering performance of the RGO LB layer can also make sure bridging a large scale and continuous sheets across interdigitated electrodes as sensing materials.

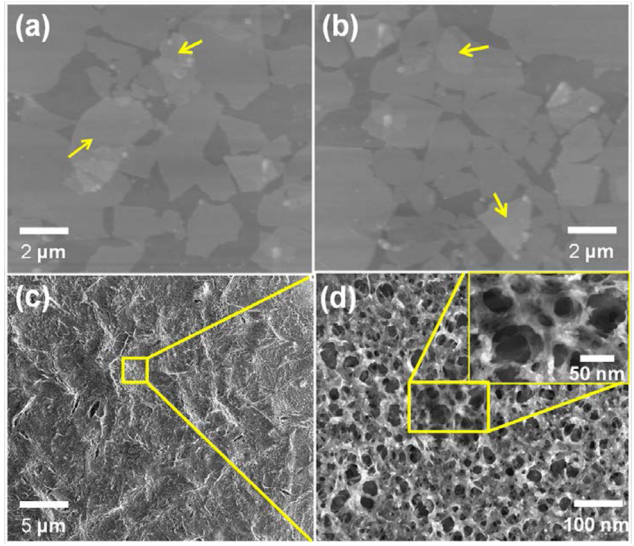

Figure 3. AFM images of (a) GO and (b) RGO LB films, and (c, d) SEM image of porous PEDOT layer deposited on RGO LB films (with a 15 °C/30 s thermal treatment speed).

The porous conducting polymer PEDOT nanostructure is constructed on RGO through the combination of in situ polymerization and a simple thermal treatment method. The RGO covered substrate is first dipped into and out slowly from the PEDOT solution, and this slow dip-coating process produces a wet PEDOT layer containing solvent on RGO. Then, this wet PEDOT layer is quickly transferred into a vacuum oven for baking, and a fast heating rate baking process is utilized to form a porous PEDOT nanostructure due to the fast volatilizing of solvent from inside the PEDOT layer. We choose *n*-butyl alcohol and acetone mixed solvent as solution for EDOT monomer polymerization. The *n*-butyl alcohol can form a stable PEDOT solution and low boiling point acetone assures the fast volatilizing of solvent from inside the PEDOT layer during the fast heating rate baking. The fast volatilizing of solvent has resulted in a bubble-like volatilization process, leading to a porous PEDOT nanostructure. By controlling the heating rates of baking, a uniformly porous PEDOT nanostructure can be obtained by this simple baking method. Figure 3c shows a SEM image of the porous PEDOT layer deposited on single layer RGO after the baking process. The PEDOT layer covered on the RGO layer exhibits a slightly fluctuate morphology after the in situ polymerization deposition. Figure 3d shows a larger magnification SEM image of porous PEDOT deposited on RGO. The uniform and well distribution of hole nanostructure in PEDOT layer is presented. As shown in Figure 3d, PEDOT layer with an average pore size about 40 nm was produced at 15 °C/30 s thermal treatment speed. The fast thermal treatment of the PEDOT layer during the polymerization results in an obviously porous PEDOT nanostructure, and this porous nanostructure also presents a uniform network formation.

As exhibited in Figure 4, a fast heating rate during the baking process results in a more uniform porous structure of PEDOT nanostructures. At a slower heating rate (1−5 °C/30 s), the obtained PEDOT layer exhibits a common and compact film morphology due to the slow volatilization of the solvent. In this baking process, we conclude that no distinct bubble-like volatilization occurred due to the slow volatilization of the solvent from inside PEDOT. However, at a faster heating rate

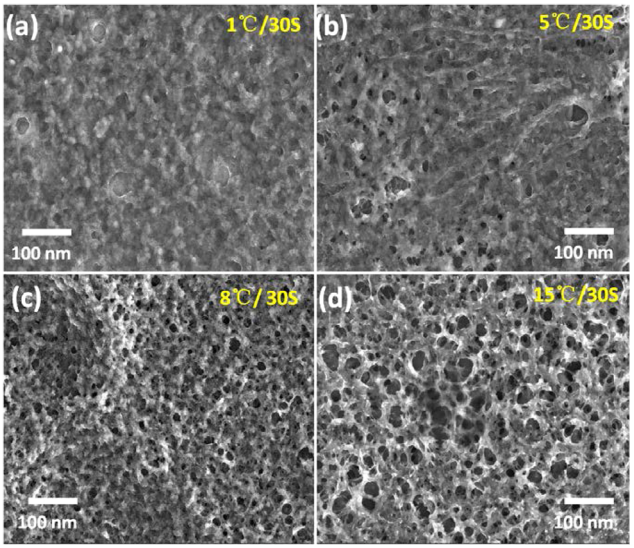

Figure 4. Influence of heating rates during baking process on porous structure of obtained PEDOT layer on RGO: (a) 1 °C/30 s, (b) 5 °C/30 s, (c) 8 °C/30 sand (d) 15 °C/30 s.

(8−15 °C/30 s), the well controlled and fast volatilizing of the solvent leads to the solvent molecules diffusing fast from the inside the PEDOT layer with a bubble-like formation, and the baked PEDOT layer exhibits an obvious porous structure. The porous PEDOT layer contains a specific surface area of about 20 m^2 g^{-1} in this work, which is comparable with the PEDOT nanoparticle (average diameter 50 nm) surface area of 29 m^2 g^{-1}. So, compared with a common PEDOT layer, the porous PEDOT structure affords a higher and highly opened surface area. Moreover, due to the direct construction of porous PEDOT on RGO, the effective specific surface area of composites is higher than that of pure porous PEDOT.

The process for preparations of GO, RGO LB films and porous PEDOT/RGO was monitored by UV−vis spectroscopy (Figure 5). The GO LB films show an absorption peak at 258

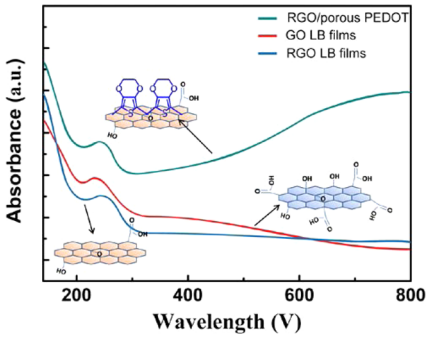

Figure 5. UV−vis-NIR spectrum of GO, RGO and RGO/porous PEDOT.

nm, and a slight red shift of this absorption peak is observed after the thermal treatment due to the reduction of GO into RGO. This result also confirms the successful reduction of GO into RGO after the thermal steam treatment, leading to the optical and conductive characteristics change of GO. After the deposition of porous PEDOT on RGO sheets, the appearance of a wide absorption peak from 600 to 800 nm derives from the polarons and bipolarons due to partly doping of PEDOT during the polymerization process.[50] This UV−vis spectrum confirms that the porous PEDOT has been successfully deposited on single layer RGO by in situ polymerization.

The FT-IR spectra of GO, RGO LB films and RGO/porous PEDOT are shown in Figure 6. The peaks located at 3458 and

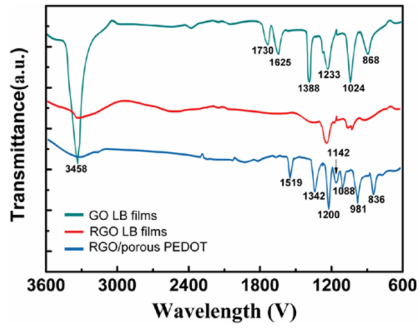

Figure 6. FT-IR spectrum of GO LB films, RGO LB films and RGO/porous PEDOT.

1388 cm^{-1} correspond to the O—H stretching and vibration mode of intercalated water. The characteristic peaks of oxygen moieties locateed at 1233, 1625 and 1730 cm^{-1} correspond to C—O (*n*(epoxy or alkoxy)), C—O in carboxylic acid and carbonyl moieties (*n*(carbonyl), respectively.[51] The featureless FT-IR spectrum of RGO indicates that the thermal reduction of GO at the water vapor environment is relatively complete with few oxygen-containing groups. From the FT-IR spectrum of RGO/porous PEDOT, the vibrational bands at about 1519 and 1342 cm^{-1} are attributed to the C═C and C—C stretching vibrations of the quininoid structure of the thiophene ring, respectively. The bands at 1200, 1142 and 1088 cm^{-1} are ascribed to the C—O—C bond stretching in the ethylene dioxy (alkylenedioxy) group. Additionally, the C—S bond in the thiophene ring is demonstrated by the presence of bands at about 981 and 836 cm^{-1}.[50] The series of bands suggests that the PEDOT is deposited on RGO through an in situ polymerization deposition.

Figure 7 shows the Raman spectra of GO LB films, RGO LB films and porous PEDOT/RGO composites. The distinctive

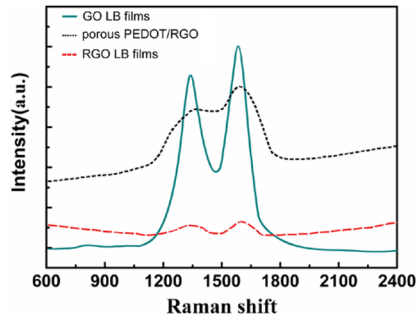

Figure 7. Raman spectra of GO LB films, RGO LB films and porous PEDOT/RGO composites.

peaks for the D bands and G bands could be observed in GO spectra. The D band located at 1345 cm^{-1}, which is a breathing mode of *k*-point phonons of A_{1g} symmetry. The G band centered at 1588 cm^{-1} is assigned to the E_{2g} phonon of C sp^2 atoms. As for RGO, the D band and G band weakened due to the reduction of GO into RGO. The spectrum of porous PEDOT/RGO shows the characteristic peaks of carbon (D band and G band), and a new shoulder peak located at 1245

cm^{-1} could be observed, which might be attributed to the valence bond between thiophene ring and RGO.[19]

The thermal steam treatment results in the reduction of GO into RGO, accompanied with structure and conductivity changes of GO. The better conductivity of RGO assures good ohmic contact between the sensing layer and electrodes. The *I*–*V* curves of GO, RGO LB films and porous PEDOT are shown in Figure 8. They indicate that a dramatic enhancement

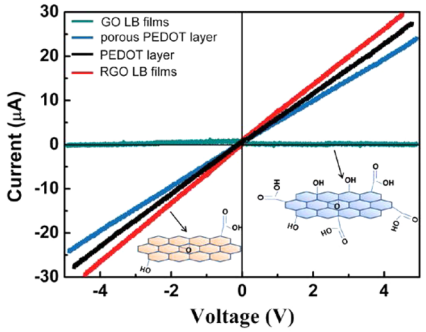

Figure 8. Current vs voltage (*I*–*V*) performance of GO LB films, RGO LB films, common PEDOT films and porous PEDOT films.

of conductivity is obtained after the thermal treatment of GO, and the successful thermal reduction of GO LB films into the RGO layer is achieved. It is well-known that the RGO exhibits tunable electrical performance depending on the reduction level of GO, and this is a useful property in sensing applications. As shown in Figure 8, the RGO LB films, common PEDOT and porous PEDOT exhibit comparable electrical performance, and the porous PEDOT shows slightly lower conductivity. It has been found that the highly reductive GO resembles graphene but, with some residual oxygen and structural defects, presents a conductivity that is comparable to doped conductive polymers.[2] The comparable electrical performance between RGO and porous PEDOT also makes sure good synergistic effect in composites and a lower noise response of composite based sensor can be achieved.

The inset of Figure 9 shows the SEM image of interdigitated electrode covered by RGO/porous PEDOT composites. Obviously, the RGO/porous PEDOT is bridging the gaps of electrodes and the porous structure sensing layer is built across the electrode arrays. The gas sensitivity of different film based sensors to NO_2 was measured according to the resistance

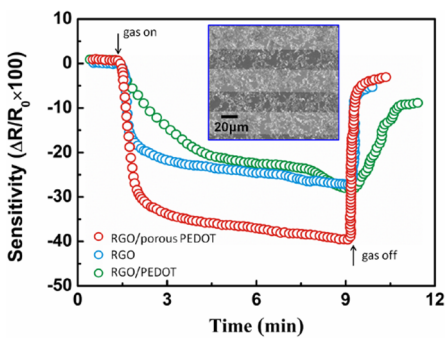

Figure 9. Gas sensitivity of different devices with RGO, RGO/PEDOT and RGO/porous PEDOT layer as sensing layers to 20 ppm of NO_2. The inset picture is the RGO/porous PEDOT covered interdigitated electrode.

change of devices after the exposure of a sensor to analyte gas. In this process, NO_2 gases with different concentration are switched into the chamber, and the resistance variations of different devices are monitored. The sensor response toward NO_2 gas was calculated according to the following equation:

$$R\ (\%) = \Delta R/R \times 100 = (R_I - R_e) \times 100/R_e \quad (1)$$

In this equation, the R_e and R_I are the resistance of RGO/porous PEDOT composite before and after exposure to NO_2 gases, respectively.

Figure 9 displays the comparison of the dynamic response of the resultant sensor based on bare RGO, RGO/PEDOT and RGO/porous PEDOT composite toward 20 ppm of NO_2 gas. As the NO_2 gas is released into the chamber, the resistances of all devices decrease. Upon exposure to NO_2 vapor, NO_2 molecules diffused into the porous PEDOT/RGO composites, and thereafter the porous PEDOT/RGO was doped. As for PEDOT, this doping process results in the introduction of a doping polymer backbone and an increase in charge carries of polarons or bipolarons. The increase of charge carries also directly gave rise to the conductivity enhancement of composites. The exposure of the device based on the RGO/porous PEDOT to NO_2 gas results in a 41.7% change of the resistance, which exhibits an obvious sensitivity 2 times that of bare RGO and common RGO/PEDOT based devices. This result suggests that a porous nanostructure constructed on RGO obviously improves the gas sensitivity of devices. Compared with pure RGO, the improvement of surface area supplying by porous PEDOT can be of benefit for the enhanced adsorption of NO_2 gas, resulting in a much better sensing performance. This obvious enhancement of sensitivity suggested that the gas sensing synergetic effects have occurred between porous PEDOT and RGO sheets, leading to a great improvement in the sensing performance.

As shown in Figure 9, both the RGO/PEDOT and bare RGO senor show fast response and recovery performance, indicating that both the bare RGO and the composite supply a highly opened surface area for fast adsorption and complete desorption of NO_2 gas. In our experiment, the response time is defined here as the time to reach 90% of the final value, and the recovery time is defined as the time needed to return to 90% of the initial steady value of the sensor-resistance. The response/recovery is also influenced by the pore size of PEDOT. As shown in Figure 9, a gas sensor based on uniform porous PEDOT/RGO with a pore size of about 40 nm exhibits a 170–180 s response time and less than 70 s recovery time to 20 ppm of NO_2 gas. The porous PEDOT/RGO not only provides a high surface-to-volume ratio but also allows rapid diffusion of analytes into and out of the composites. For a common RGO/PEDOT composite, no obvious improvement of gas sensitivity is observed after the deposition of a common PEDOT layer on RGO. The sensor based on the common RGO/PEDOT composite is also difficult to saturate. A longer period is needed to remove the absorbed NO_2 gas and reach the steady state, and this steady state also shows incomplete recovery to initial resistance. We conclude that a complete and compact covering of PEDOT on RGO results in the loss of a highly open surface area of RGO during the sensing process. The compact PEDOT film structure gives rise to slower adsorption and desorption speeds of gas molecules, especially at the interface between RGO and PEDOT. However, almost complete recovery to initial resistance of the device is achieved for RGO/porous PEDOT based gas sensors. Due to the highly opened surface

area of RGO sheets and the porous PEDOT nanostructure, a shorter recovery period is presented for the sensing device based on this composite. We also investigated the performance of porous PEDOT/RGO, RGO and common RGO/PEDOT based gas sensor in a synthetic air. In a synthetic air, the porous PEDOT/RGO also exhibited the best and stable sensing performance of the three kinds of sensing materials. A slight decrease in sensitivity to NO_2 gas is observed due to the adsorption of other gases.

As shown in Figure 10, we investigated the influence of porous morphology in PEDOT on the gas sensing performance

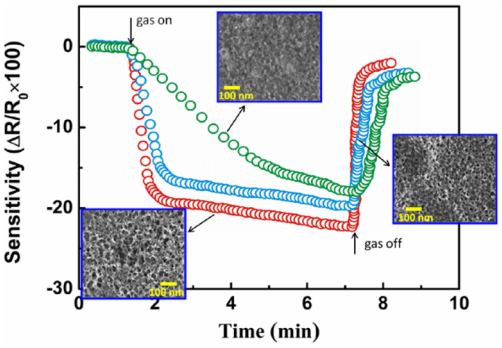

Figure 10. Influence of porous structure on gas sensitivity of RGO/porous PEDOT based gas sensor to 5 ppm of NO_2.

of RGO/porous PEDOT based gas sensors. It is obvious that the sensor based on RGO/porous PEDOT composites containing larger size holes and the uniform distribution of holes exhibits the best sensing performance. During the long time exposure of a sensor to 5 ppm of NO_2 gas, this device shows fast response and recovers to the initial state rapidly after cutting off the analyte gas. It is postulated that the uniform distribution of the nanoporous structures in PEDOT tremendously improves the adsorption and desorption speed of gas molecules during the sensing process. However, the porous PEDOT layer contains less and the unordered hole distribution is more like a common PEDOT layer. The common RGO/PEDOT composite based sensor exhibits long response and recovery time due to the inferior surface structure for gas molecule adsorption and desorption.

The repeatability of the RGO/porous PEDOT based gas sensor is shown in Figure 11. Five cycles of responses to NO_2 gas have been executed through exposure of the composite based sensor to 5 ppm of NO_2 gas repeatedly. The sensor

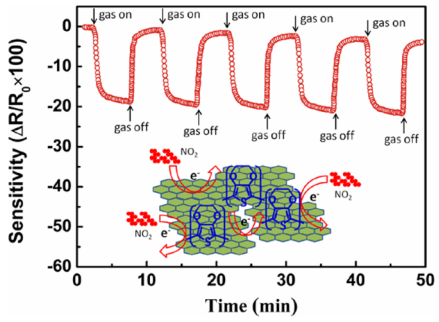

Figure 11. Repeatable characteristic of RGO/porous PEDOT based sensor to 2 ppm of NO_2 gas and schematic illustration of interaction between NO_2 and composites.

exhibits an excellent repeatable characteristic, and the response levels of the sensor can be maintained after repeated cycles. For gas sensing detection, RGO exhibits p-type or n-type behavior depending on the oxidant characteristics of ayalyte gas. As for NO_2, a strong oxidant and toxic gas, RGO prefer to exhibit the p-type behavior after the exposure to NO_2, which means that the RGO would donate electrons to NO_2 molecules during the sensing interactions. The exposure of RGO sheets to NO_2 gas causes an increase in the number of charge carriers, resulting in resistance decrease in the composites. As for the conducting polymer PEDOT, it mostly exhibits the p-type behavior to NO_2 and the exposure of porous PEDOT to NO_2 would tremendously decrease the resistance of the RGO/PEDOT composite. Compared with pure PEDOT or RGO, the accumulation of resistance change caused by RGO and porous PEDOT spontaneously results in the enhancement of sensitivity of composites based gas sensor. Moreover, as a stable conducting polymer, PEDOT can interact with RGO sheets through p−p interaction at the interface of RGO and porous PEDOT. The Raman and FT-IR analysis confirms that p−p interaction is formed between the porous PEDOT and RGO. This p−p interaction also can cause a charge carriers increase, resulting in the resistance decrease of composites. We conclude that this p−p interaction between PEDOT and RGO is partly ascribed to the sensitivity improvement of gas sensor. So, due to the excellent synergistic effect, this single layer RGO/porous PEDOT nanocomposite afford excellent reproducing stability to toxic NO_2, especially for stable detection of lower concentration NO_2 gas.

Figure 12 shows the response of the sensor device based on RGO/porous PEDOT to different concentrations of NO_2 gases

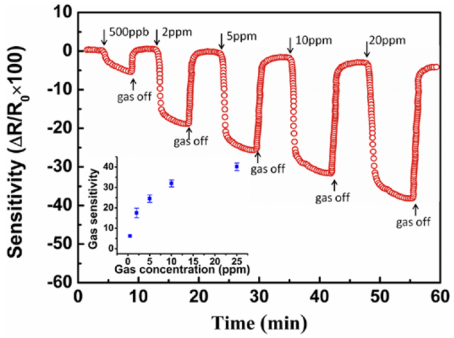

Figure 12. Sensitivity of RGO/porous PEDOT based device to different concentrations of NO_2 gas.

at room temperature. During the exposure of the device to different concentrations of NO_2 gas, the obvious resistance change can be achieved for gas concentrations from 500 ppb to 20 ppm. The results indicate that, even at the ppb level, the RGO/porous PEDOT based sensing device exhibits a fast response and recovery performance. With increases of the NO_2 gas concentration, the resistance of the device increases accordingly. The RGO/porous PEDOT nanostrucrure based gas sensors show promising application as a candidate for actual NO_2 gas detection in atmosphere conditions.

The influence of relative humidity (RH) on sensing performance of the porous PEDOT/RGO based gas sensor is also investigated, which is shown in Figure 13. The presence of humidity leads primarily to a shift of the baseline of the sensor. The sensor performance is not disturbed obviously, and the

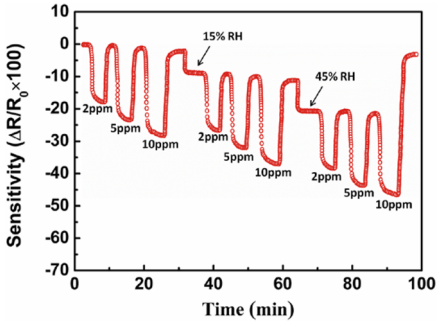

Figure 13. Influence of relative humidity (RH) on gas sensor performance to 2, 5 and 10 ppm of NO_2 gas.

dynamic response range of the sensor decreases slightly with the increase of humidity.

As promising gas sensing materials, RGO affords the high surface area and low noise response for gas detection. But the high selectivity of a bare RGO based gas sensor is still a challenge, especially for low concentration gas detection. So, we investigate the selectivity of this RGO/porous PEDOT composite based sensor. As shown in Figure 14, NO_2 gas has

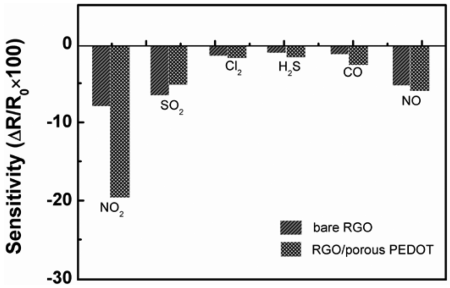

Figure 14. Gas selectivity of bare RGO and RGO/porous PEDOT based device to 2 ppm different analyte gases.

been used for the evaluation of the sensor through the comparison with other analyte gases, e.g., HCl, H_2S and SO_2, in the same concentrations. The RGO/porous PEDOT gas senor shows an obviously high selectivity to 2 ppm of NO_2 compared with other analyte gases. The high selectivity of the RGO/porous PEDOT based gas sensor demonstrates this composite is an excellent candidate for the detection of NO_2 gas in complicated gas environments. In Figure 14, the sensing performance of the sensor based on RGO/porous PEDOT has been also compared to that of gas sensor based on bare RGO. The gas sensor based on the RGO/porous PEDOT exhibits much higher response than that of the gas sensor based on bare RGO. The construction of porous PEDOT nanostructure on single layer RGO has tremendously increased the sensing selectivity of a gas sensor to low concentrations of NO_2 gas. The excellent synergetic effect of RGO and porous PEDOT during the sensing process of nanocomposites is attributed to this selectivity improvement.

4. CONCLUSIONS

A single layer RGO layer and porous PEDOT nanocomposite has been successfully prepared by LB deposition and an in situ polymerization method. The porous PEDOT nanostructure is constructed on RGO LB films through a fast heating rate baking during the in situ solution polymerization of EDOT. The high surface area and porous nanostructure of this novel nanocomposite enhance gas adsorption and desorption. The results of gas sensing performance indicate that the RGO/porous PEDOT composite based device exhibits excellent sensing performance to NO_2 gas compared with those of the sensors based on bare RGO and common RGO/PEDOT. The porous nanostructure of conducting polymer PEDOT constructed on RGO shows promising applications for high performance gas sensors due to the tremendous enhancement of sensitivity and selectivity of the gas sensor at the ppb level detection of toxic NO_2 gas.

AUTHOR INFORMATION

Corresponding Author

*S. Li. E-mail: shibinli@uestc.edu.cn. Tel: +86-28-83208959. Fax: +86-28-83206123.

Notes

The authors declare no competing financial interest.

ACKNOWLEDGMENTS

The work was supported by the National Science Foundation of China (NSFC) (Nos. 61101029 and 61371046), a plan funding for supporting the New Century Talents (No. NCET-12-0091) and Projects of International Cooperation and Exchanges of Sichuan Province (No. 2014HH0041).

REFERENCES

(1) Zhu, Y. W.; Murali, S.; Cai, W. W.; Li, X. S.; Suk, J. W.; Potts, J. R.; Ruof, R. S. Graphene and Graphene Oxide: Synthesis, Properties, and Applications. *Adv. Mater.* **2010**, *22*, 3906−3924.

(2) Dreyer, D. R.; Park, S.; Bielawski, C. W.; Ruof, R. S. The Chemistry of Graphene Oxide. *Chem. Soc. Rev.* **2010**, *39*, 228−240.

(3) Wan, X. J.; Huang, Y.; Chen, Y. S. Focusing on Energy and Optoelectronic Applications: A Journey for Graphene and Graphene Oxide at Large Scale. *Acc. Chem. Res.* **2012**, *45*, 598−607.

(4) Chen, D.; Fengand, H. B.; Li, J. H. Graphene Oxide: Preparation, Functionalization, and Electrochemical Applications. *Chem. Rev.* **2012**, *112*, 6027−6053.

(5) Compton, O. C.; Nguyen, S. T. Graphene Oxide, Highly Reduced Graphene Oxide, and Graphene: Versatile Building Blocks for Carbon-based Materials. *Small* **2010**, *6*, 711−723.

(6) Zhou, M.; Zhai, Y. M.; Dong, S. J. Electrochemical Sensing and Biosensing Platform Based on Chemically Reduced Graphene Oxide. *Anal. Chem.* **2009**, *81*, 5603−5613.

(7) Eda, G.; Chhowalla, M. Chemically Derived Graphene Oxide: Towards Large-Area Thin-Film Electronics and Optoelectronics. *Adv. Mater.* **2010**, *22*, 2392−2415.

(8) Zhang, L. M.; Xia, J. G.; Zhao, Q. H.; Liu, L. W.; Zhang, Z. J. Functional Graphene Oxide as a Nanocarrier for Controlled Loading and Targeted Delivery of Mixed Anticancer Drugs. *Small* **2010**, *6*, 537−544.

(9) Yang, X. Y.; Zhang, X. Y.; Liu, Z. F.; Ma, Y. F.; Huang, Y.; Chen, Y. S. High-Efficiency Loading and Controlled Release of Doxorubicin Hydrochloride on Graphene Oxide. *J. Phys. Chem. C* **2008**, *112*, 17554−17558.

(10) Robinson, J. T.; Perkins, F. K.; Snow, E. S.; Wei, Z. Q.; Sheehan, P. E. Reduced Graphene Oxide Molecular Sensors. *Nano Lett.* **2008**, *8*, 3137−3140.

(11) Dikin, D. A.; Stankovich, S.; Zimney, E. J.; Piner, R. D.; Dommett, G. H. B.; Evmenenko, G.; Nguyen, S. T.; Ruoff, R. S. Preparation and Characterization of Graphene Oxide Paper. *Nature* **2007**, *448*, 457−460.

(12) Shen, J. F.; Hu, Y. Z.; Shi, M.; Lu, X.; Qin, C.; Li, C.; Ye, M. X. Fast and Facile Preparation of Graphene Oxide and Reduced Graphene Oxide Nanoplatelets. *Chem. Mater.* **2009**, *21*, 3514−3520.

(13) Stankovich, S.; Dikin, D. A.; Piner, R. D.; Kohlhaas, K. A.; Kleinhammes, A.; Jia, Y. Y.; Wu, Y.; Nguyen, S. T.; Ruoff, R. S.

Synthesis of Graphene-based Nanosheets via Chemical Reduction of Exfoliated Graphite Oxide. *Carbon* **2007**, *45*, 1558−1565.
(14) Kuilla, T.; Bhadra, S.; Yao, D.; Kim, N. H.; Bose, S.; Lee, J. H. Recent Advances in Graphene Polymer Composites. *Prog. Polym. Sci.* **2010**, *35*, 1350−1375.
(15) Cote, L. J.; Cruz-Silva, R.; Huang, J. X. Flash Reduction and Patterning of Graphite Oxide and Its Polymer Composite. *J. Am. Chem. Soc.* **2009**, *131*, 11027−11032.
(16) Zhu, X. J.; Zhu, Y. W.; Murali, S.; Stoller, M. D.; Ruoff, R. S. Nano Structured Reduced Graphene Oxide/Fe_2O_3 Composites as High Performance Anode Materials for Lithium Ion Batteries. *ACS Nano* **2011**, *5*, 3333−3338.
(17) Gómez-Navarro, C.; Weitz, R. T.; Bittner, A. M.; Scolari, M.; Mews, A.; Burghard, M.; Kern, K. Electronic Transport Properties of Individual Chemically Reduced Graphene Oxide Sheets. *Nano Lett.* **2007**, *7*, 3499−3503.
(18) Jung, I.; Dikin, D. A.; Piner, R. D.; Ruoff, R. S. Tunable Electrical Conductivity of Individual Graphene Oxide Sheets Reduced at "Low" Temperatures. *Nano Lett.* **2008**, *8*, 4283−4287.
(19) Pei, S. F.; Cheng, H. M. The Reduction of Graphene Oxide. *Carbon* **2012**, *50*, 3210−3228.
(20) Kim, F.; Cote, L. J.; Huang, J. X. Graphene Oxide, Surface Activity and Two-Dimensional Assembly. *Adv. Mater.* **2010**, *22*, 1954−1958.
(21) Zhang, J. L.; Yang, H. J.; Shen, G. X.; Cheng, P.; Zhang, J. Y.; Guo, S. W. Reduction of Graphene Oxide via L-Ascorbic Acid. *Chem. Commun.* **2010**, *46*, 1112−1114.
(22) Wei, Z. Q.; Wang, D. B.; Kim, S.; Kim, S. Y.; Hu, Y. K.; Yakes, M. K.; Laracuente, A. R.; Dai, Z. T.; Marder, S. R.; Berger, C.; King, W. P.; de Heer, W. A.; Sheehan, P. E.; Riedo, E. Nanoscale Tunable Reduction of Graphene Oxide for Graphene Electronics. *Science* **2010**, *328*, 1373−1376.
(23) Zhang, J. T.; Zhao, X. S. Conducting Polymers Directly Coated on Reduced Graphene Oxide Sheets as High-Performance Supercapacitor Electrodes. *J. Phys. Chem. C* **2012**, *116*, 5420−5426.
(24) Zhang, L. L.; Zhao, S. Y.; Tian, X. N.; Zhao, X. S. Layered Graphene Oxide Nanostructures with Sandwiched Conducting Polymers as Supercapacitor Electrodes. *Langmuir* **2010**, *26*, 17624−17628.
(25) Wang, D. W.; Li, F.; Zhao, J. P.; Ren, W. C.; Chen, Z. G.; Tan, J.; Wu, Z. S.; Gentle, I.; Lu, G. Q.; Cheng, H. M. Fabrication of Graphene/Polyaniline Composite Paper via In Situ Anodic Electropolymerization for High-Performance Flexible Electrode. *ACS Nano* **2009**, *3*, 1745−1752.
(26) Eda, G.; Fanchini, G.; Chhowalla, M. Large-Area Ultrathin Films of Reduced Graphene Oxide as a Transparent and Flexible Electronic Material. *Nat. Nanotechnol.* **2008**, *3*, 270−274.
(27) Yin, Z. Y.; Wu, S. X.; Zhou, X. Z.; Huang, X.; Zhang, Q. C.; Boey, F.; Zhang, H. Electrochemical Deposition of ZnO Nanorods on Transparent Reduced Graphene Oxide Electrodes for Hybrid Solar Cells. *Small* **2010**, *6*, 307−312.
(28) Fan, W. F.; Lai, Q. H.; Zhang, Q. H.; Wang, Y. Nanocomposites of TiO_2 and Reduced Graphene Oxide as Efficient Photocatalysts for Hydrogen Evolution. *J. Phys. Chem. C* **2011**, *115*, 10694−10701.
(29) Schedin, F.; Geim, A. K.; Morozov, S. V.; Hill, E. W.; Blake, P.; Katsnelson, M. I.; Novoselov, K. S. Detection of Individual Gas Molecules Adsorbed on Rraphene. *Nat. Mater.* **2007**, *6*, 652−655.
(30) Hua, N. T.; Wang, Y. Y.; Chai, J.; Gao, R. G.; Yang, Z.; Kong, E. S. W.; Zhang, Y. F. Gas Sensor Based on p-Phenylenediamine Reduced Graphene Oxide. *Sens. Actuators, B* **2012**, *163*, 107−114.
(31) Hu, N. T.; Yang, Z.; Wang, Y. Y.; Zhang, L. L.; Wang, Y.; Huang, X. L.; Wei, H.; Wei, L. M.; Zhang, Y. F. Ultrafast and Sensitive Room Temperature NH_3 Gas Sensors Based on Chemically Reduced Graphene Oxide. *Nanotechnology* **2014**, *25*, 025502.
(32) Yuan, W. J.; Liu, A. R.; Huang, L.; Li, C.; Shi, G. Q. High-Performance NO_2 Sensors Based on Chemically Modified Graphene. *Adv. Mater.* **2013**, *25*, 766−771.
(33) Lu, G. H.; Ocola, L. E.; Chen, J. H. Reduced Graphene Oxide for Room-Temperature Gas Sensors. *Nanotechnology* **2009**, *20*, 445502.
(34) Lu, G. H.; Ocola, L. E.; Chen, J. H. Gas Detection Using Low-Temperature Reduced Graphene Oxide Sheets. *Appl. Phys. Lett.* **2009**, *94*, 083111−083113.
(35) Jeong, H. Y.; Lee, D. S.; Choi, H. K.; Lee, D. H.; Kim, J. E.; Lee, J. Y.; Lee, W. J.; Kim, S. O.; Choi, S. Y. Flexible Room-Temperature NO_2 Gas Sensors Based on Carbon Nanotubes/Reduced Graphene Hybrid Films. *Appl. Phys. Lett.* **2010**, *96*, 213105−213108.
(36) Han, T. H.; Huang, Y. K.; Tan, A. T. L.; Dravid, V. P.; Huang, J. X. Steam Etched Porous Graphene Oxide Network for Chemical Sensing. *J. Am. Chem. Soc.* **2011**, *133*, 15264−15267.
(37) Dua, V.; Surwade, S. P.; Ammu, S.; Agnihotra, S. R.; Jain, S.; Roberts, K. E.; Park, S.; Ruoff, R. S.; Manohar, S. K. All-Organic Vapor Sensor Using Inkjet-Printed Reduced Graphene Oxide. *Angew. Chem., Int. Ed.* **2010**, *49*, 2154−2157.
(38) Myers, M.; Cooper, J.; Pejcic, B.; Baker, M.; Raguse, B.; Wieczorek, L. Functionalized Graphene as an Aqueous Phase Chemiresistor Sensing Material. *Sens. Actuators, B* **2011**, *155*, 154−158.
(39) Bai, H.; Shi, G. Q. Gas Sensors Based on Conducting Polymers. *Sensors* **2007**, *7*, 267−307.
(40) Jang, J.; Chang, M.; Yoon, H. Chemical Sensors Based on Highly Conductive Poly(3,4-ethylenedioxythiophene) Nanorods. *Adv. Mater.* **2005**, *17*, 1616−1620.
(41) Hatchett, D. W.; Josowicz, M. Composites of Intrinsically Conducting Polymers as Sensing Nanomaterials. *Chem. Rev.* **2008**, *108*, 746−769.
(42) Huang, X. L.; Hu, N. T.; Gao, R. G.; Yu, Y.; Wang, Y. Y.; Yang, Z.; Kong, E. S. W.; Wei, H.; Zhang, Y. F. Reduced Graphene Oxide−Polyaniline Hybrid: Preparation, Characterization and Its Applications for Ammonia Gas Sensing. *J. Mater. Chem.* **2012**, *22*, 22488−22495.
(43) Basu, S.; Bhattacharyya, P. Recent Developments on Graphene and Graphene Oxide based Solid State Gas Sensors. *Sens. Actuators, B* **2012**, *173*, 1−21.
(44) Chandra, V.; Yu, S. U.; Kim, S. H.; Yoon, Y. S.; Kim, D. Y.; Kwon, A. H.; Meyyappan, M.; Kim, K. S. Highly Selective CO_2 Capture on N-Doped Carbon Produced by Chemical Activation of Polypyrrole Functionalized Graphene Sheets. *Chem. Commun.* **2012**, *48*, 735−737.
(45) Saleh, M.; Tiwari, J. N.; Kemp, K. C.; Yousuf, M.; Kim, K. S. Highly Selective and Stable Carbon Dioxide Uptake in Polyindole-Derived Microporous Carbon Materials. *Environ. Sci. Technol.* **2013**, *47*, 5467−5473.
(46) Kemp, K. C.; Chandra, V.; Saleh, M.; Kim, K. S. Reversible CO_2 Adsorption by an Activated Nitrogen Doped Graphene/Polyaniline Material. *Nanotechnology* **2013**, *24*, 235703.
(47) Kuila, T.; Bose, S.; Mishra, A. K.; Khanra, P.; Kim, N. H.; Lee, J. H. Chemical Functionalization of Graphene and Its Applications. *Prog. Mater. Sci.* **2012**, *57*, 1061−1105.
(48) Ratinac, K. R.; Yang, W. R.; Gooding, J. J.; Thordarson, P.; Braet, F. Graphene and Related Materials in Electrochemical Sensing. *Electroanalysis* **2011**, *23*, 803−826.
(49) Hummers, W. S.; Offeman, R. E. Preparation of Graphitic Oxide. *J. Am. Chem. Soc.* **1958**, *80*, 1339−1339.
(50) Yang, Y. J.; Jiang, Y. D.; Xu, J. H.; Yu, J. S. Conducting Polymeric Nanoparticles Synthesized in Reverse Micelles and Their Gas Sensitivity Based on Quartz Crystal Microbalance. *Polymer* **2007**, *48*, 4459−4465.
(51) Chen, W. F.; Yan, L. F.; Bangal, P. R. Chemical Reduction of Graphene Oxide to Graphene by Sulfur-Containing Compounds. *J. Phys. Chem. C* **2010**, *114*, 19885−19890.